

# NIH RELAIS Document Delivery

NIH-10286735

JEFFDUYN

NIH -- W1 MA34IF

JOZEF DUYN  
10 Center Dirve  
Bldg. 10/Rm.1L07  
Bethesda, MD 20892-1150

ATTN: SUBMITTED: 2002-08-29 17:22:17  
PHONE: 301-594-7305 PRINTED: 2002-09-03 07:24:39  
FAX: - REQUEST NO.: NIH-10286735  
E-MAIL: SENT VIA: LOAN DOC  
7967412

---

NIH	Fiche to Paper	Journal
TITLE:	MAGNETIC RESONANCE IN MEDICINE : OFFICIAL JOURNAL OF THE SOCIETY OF MAGNETIC RESONANCE IN MEDICINE / SOCIETY OF MAGNETIC RESONANCE IN MEDICINE	
PUBLISHER/PLACE:	Wiley-Liss, Inc., a division of John Wil New York, NY :	
VOLUME/ISSUE/PAGES:	1996 Aug;36(2):217-24 217-24	
DATE:	1996	
AUTHOR OF ARTICLE:	Ye FQ; Pekar JJ; Jezzard P; Duyn J; Frank JA; McLaughlin AC	
TITLE OF ARTICLE:	Perfusion imaging of the human brain at 1.5 T usin	
ISSN:	0740-3194	
OTHER NOS/LETTERS:	Library reports holding volume or year 8505245 8843375	
SOURCE:	PubMed	
CALL NUMBER:	W1 MA34IF	
REQUESTER INFO:	JEFFDUYN	
DELIVERY:	E-mail: jhd@helix.nih.gov	
REPLY:	Mail:	

NOTICE: THIS MATERIAL MAY BE PROTECTED BY COPYRIGHT LAW (TITLE 17, U.S. CODE)

---National-Institutes-of-Health,-Bethesda,-MD-----

# Perfusion Imaging of the Human Brain at 1.5 T Using a Single-Shot EPI Spin Tagging Approach

Frank Q. Ye, James J. Pekar, Peter Jezzard, Jeff Duyn, Joseph A. Frank, Alan C. McLaughlin

Single-shot echo planar imaging (EPI) techniques have been applied, in conjunction with arterial spin tagging approaches, to obtain images of cerebral blood flow in a single axial slice in the human brain. Serial studies demonstrate that cerebral blood flow images acquired in 8 min are reproducible, with a statistical precision of approximately  $\pm 10$  cc/100 g/min. The average value of cerebral blood flow in the slice is  $51 \pm 11$  cc/100 g/min for six normal subjects. The cerebral blood flow images contain two types of artifact, probably due to arterial and venous blood volume contributions, which must be overcome before the arterial spin tagging approach can be used for routine clinical studies.

**Key words:** cerebral blood flow; perfusion; human; brain.

## INTRODUCTION

Arterial "spin tagging" approaches (1) have recently been used to image cerebral blood flow in rodents (1–4), cats (5), and humans (6, 7). These approaches estimate cerebral blood flow,  $Q$ , using the equation

$$\Delta M/M_0 = \frac{-2\alpha Q/\lambda}{1/T_1}$$

where  $\Delta M/M_0$  is the fractional change in steady-state longitudinal water magnetization in the brain when arterial water spins are inverted,  $\alpha$  is the degree of inversion of arterial water spins,  $\lambda$  is the brain/blood partition coefficient for water, and  $1/T_1$  is the longitudinal relaxation rate of brain water spins.

One advantage of arterial spin tagging approaches is that the data can be interpreted using classical tracer theory to give quantitative estimates of cerebral blood flow. A disadvantage is that the small observed changes in longitudinal magnetization, e.g.,  $\sim 2\%$  in humans at 1.5 T (6, 7), make the approach very sensitive to experimental instabilities and head motion. The sensitivity to experimental instabilities can be minimized by using fast imaging techniques. In this communication we demonstrate that single-shot echo planar imaging (EPI) techniques (8–10) can be used with arterial spin tagging

approaches to obtain reproducible perfusion images of the human head.

## MATERIALS AND METHODS

### Experimental Protocol

Experiments were performed on six normal subjects (three males and three females), using a protocol approved by the Institutional Review Board of the National Institute of Mental Health.

Twenty-three sagittal images covering the entire head were acquired to localize the slice used for perfusion imaging. An axial slice approximately 1 cm above the corpus callosum was chosen, and spin echo (SE) and flow-compensated spoiled grass (SPGR) images of this slice acquired.

EPI approaches (see below) were then used to obtain at least six images of  $\Delta M/M_0$  (5) for the chosen slice, each using a different value of  $\gamma B_1$ , the amplitude of the off-resonance RF irradiation (see Fig. 1). Using this data, a value of  $\gamma B_1$  for the spin tagging experiments was chosen (see below).

Finally, spin tagging approaches were used to obtain perfusion images of the axial slice. A typical spin tagging experiment involved the acquisition of three perfusion images. Each perfusion image was calculated from the data contained in a single pair of images. The first image in the pair was a  $T_1$  image, which took approximately 3 min to acquire. The second was a  $\Delta M/M_0$  image (5), which took approximately 5 min to acquire.

### MR Imaging

All experiments were performed on a 1.5 T (General Electric, Milwaukee, WI) scanner employing a 3-axis local gradient head coil (Medical Advances, Milwaukee, WI). The rise time for the gradients was 200  $\mu$ s and the maximum gradient strength was 2 Gauss/cm.

Spin echo EPI images were obtained using a  $64 \times 64$  matrix, a 24-cm field of view, a slice thickness of 5 mm,  $TE = 60$  ms,  $TR = 2$  s. Strong gradients (0.6 ms, 1.7 Gauss/cm) were placed symmetrically around the  $180^\circ$  pulse to "crush" signals from arterial water spins (5). The  $T_1$  relaxation rate for each voxel in the EPI image was determined using an inversion recovery sequence with EPI readout. Sixteen TI values, uniformly distributed between 0.2 and 3.2 s, were used.  $TR$  was 8 s. The entire  $T_1$  measurement was completed in 154 s.  $T_1$  was calculated using a three-parameter fit to the data.

Anatomical images of the imaging slice were acquired using a spin echo sequence with a  $256 \times 256$  matrix and a slice thickness of 5 mm, with  $TE = 20$  ms and  $TR = 500$  ms. Flow sensitive "angiographic" images of the imaging

### MRM 36:219–224 (1996)

From the Clinical Brain Disorders Branch, NIMH, NIH, (F.Q.Y., A.C.M.), the Laboratory of Diagnostic Radiology Research, OIR, NIH, (J.J.P., J.D., J.A.F.), and the Laboratory of Psychology and Psychopathology, NIMH, NIH, Bethesda, Maryland (P.J.); and the Institute for Cognitive and Computational Sciences, Georgetown University Medical Center, Washington, D.C. (J.J.P.).

Address correspondence to: Alan C. McLaughlin, Ph.D., Building 10; Room B1D-125, National Institutes of Health, Bethesda, MD 20892-1060.

Received October 30, 1995; revised January 17, 1996; accepted February 27, 1996.

0740-3194/96 \$3.00

Copyright © 1996 by Williams & Wilkins

All rights of reproduction in any form reserved.

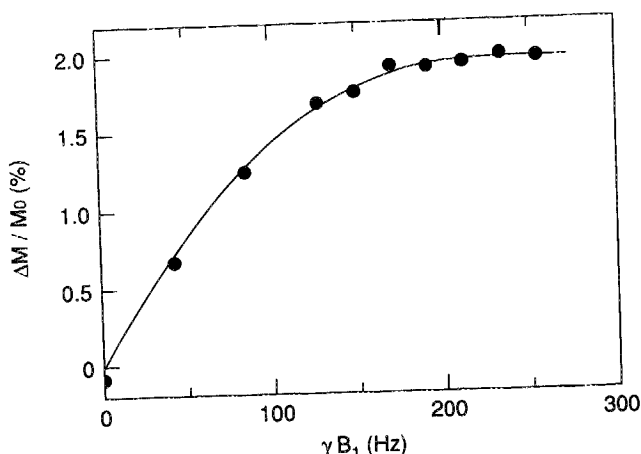


FIG. 1. Dependence of  $\Delta M/M_0$ , the fractional change in longitudinal magnetization for a brain ROI, as a function of the amplitude of the off-resonance RF irradiation,  $\gamma B_1$ . The ROI contained all of the brain tissue in the imaging slice. The solid curve through the data points has no theoretical significance.

slice were acquired using a flow-compensated SPGR sequence with a  $512 \times 512$  matrix and a slice thickness of 3 mm, with  $TE = 17$  ms,  $TR = 55$  ms,  $\theta = 60^\circ$ . Five SPGR images were acquired, centered around the slice chosen for the cerebral blood flow image.

#### Spin Tagging

Flow-induced adiabatic inversion (2) was used to invert arterial water spins flowing through the "tagging" plane. Inversion was accomplished using a 1.8 s off-resonance RF pulse train in the presence of a  $z$  gradient. The pulse train consisted of rectangular RF pulses of 75 ms duration separated by 10 ms. The amplitude of the off-resonance RF field was calibrated by measuring the width of a rectangular (on-resonance) RF pulse that produced a  $90^\circ$  nutation. The frequency offset of the irradiating RF pulse ( $\pm 4000$  Hz) and the sign of the  $z$  gradient ( $\pm 200$  Hz/mm) were alternated in a four-step protocol to minimize the influence of asymmetric magnetization transfer effects and gradient eddy currents (5).  $\Delta M/M_0$  was calculated from the data, according to the procedure outlined previously (5). In essence, this procedure averages two values of  $\Delta M/M_0$ : one value of  $\Delta M/M_0$  was calculated using a gradient inversion with  $\Delta\omega = +4000$  Hz, while the second was calculated using a gradient inversion with  $\Delta\omega = -4000$  Hz. The data from 39 four-step cycles were averaged to obtain a single  $\Delta M/M_0$  image, which was acquired in approximately 5 min. The amplitude of the off-resonance RF irradiation,  $\gamma B_1$ , was chosen so that further increases in  $\gamma B_1$  did not give measurable increases in  $\Delta M/M_0$  (see Fig. 1). A typical value of  $\gamma B_1$  was 170 Hz.

The "nominal" resolution of the  $64 \times 64$  cerebral blood flow images, i.e., the resolution calculated ignoring the effect of relaxation on the point-spread function, was 3.75 mm. However, for visual presentation, cerebral blood flow images were interpolated with zeros from  $64 \times 64$  to  $512 \times 512$ , and convolved with a two-dimensional Gaussian kernel having a full-width-at-half-height of 5.3 mm. The "nominal" spatial resolution of the result-

ing  $512 \times 512$  image, calculated from computer simulations of the effect of interpolation and convolution on the point-spread function, was 5.8 mm.

## RESULTS

### Calculation of Cerebral Blood Flow Images

Figure 2a shows a sagittal image indicating the location of the tagging plane and the imaging slice for a typical cerebral blood flow experiment. Figure 2b shows an SE ("anatomical") image, and Fig. 2c shows a SPGR ("angiographic") image of this slice. Figure 2d shows an image of  $T_1$  relaxation times in the slice, and Fig. 3 is a histogram of the values from the  $T_1$  image.

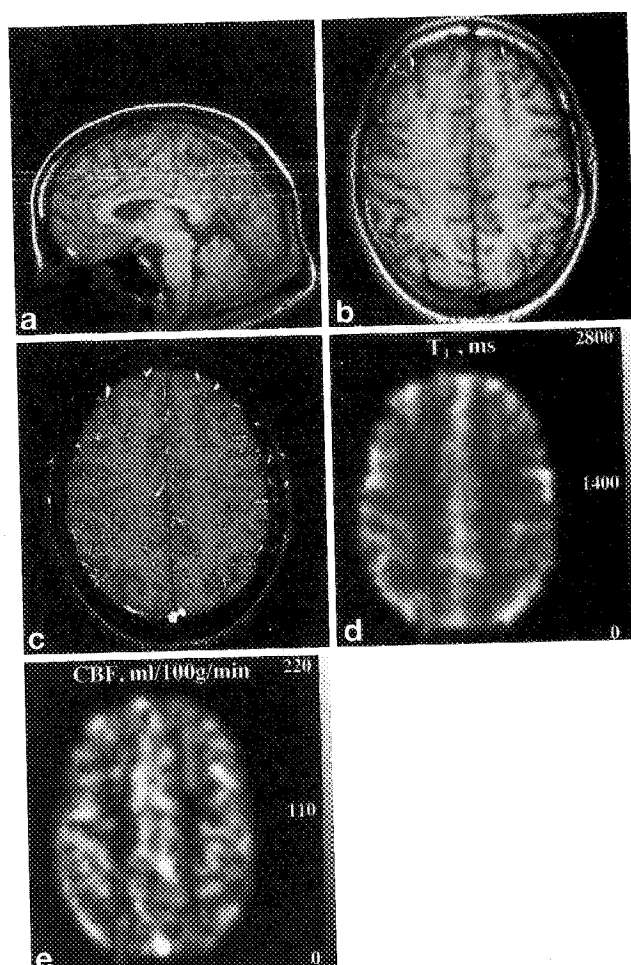


FIG. 2. (a) Sagittal image of a human head, showing the location of the imaging slice (solid lines) and the inversion plane (dashed line) used for the perfusion imaging experiments. Distortion of the image at the bottom of the head is due to nonlinearity of the gradient insert coil in this region. (b) Anatomical image of the slice outlined in (a). The image was acquired using a spin echo sequence with  $TE = 20$  ms and  $TR = 500$  ms. (c) "Angiographic" image of the slice outlined in (a). The image was acquired using a flow-compensated spoiled grass (SPGR) sequence with  $TE = 17$  ms,  $TR = 55$  ms,  $\theta = 60^\circ$ . (d) Image of  $T_1$  relaxation times of brain water in the slice shown in (b). (e) Image of cerebral blood flow values for the slice shown in (b). Negative cerebral blood flow values (see text) were replaced by zero before the image was interpolated and Gaussian "smoothed."

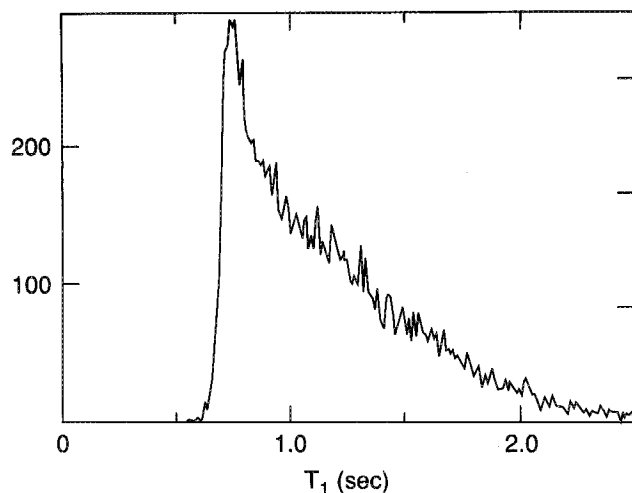


FIG. 3. Histogram of  $T_1$  relaxation times from the image shown in Fig. 2e. The vertical scale corresponds to the number of voxels having a specific  $T_1$  relaxation time. A 10-ms range was used to "bin" the  $T_1$  data.

An image of  $\Delta M/M_0$  was obtained using the four-step protocol described previously (5). Cerebral blood flow was calculated using Eq. [1] and the values of  $\Delta M/M_0$  and  $1/T_1$  in each voxel, assuming that  $\alpha = 1$ . Complete arterial inversion (i.e.,  $\alpha = 1$ ) was assumed because increases in the amplitude of the off-resonance RF irradiation,  $\gamma B_1$ , did not result in an increase in  $\Delta M/M_0$  (see Fig. 1) (5). This assumption ignores the decrease in  $\alpha$  due to longitudinal relaxation during transit from the tagging plane to tissue in the imaging slice (see Fig. 2a), which will result in an under-estimate of cerebral blood flow (5). This transit time has been estimated to be  $\sim 0.2$  s (6), which would give a decrease in  $\alpha$  of  $\sim 15\%$ .  $\lambda$  was assumed to be 0.90 ml/g (11).

Figure 2e is an image of cerebral blood flow in the slice indicated in Fig. 2a. The image clearly shows regions of high and low flow that correlate with gray and white matter regions outlined in the high-resolution anatomical image (Fig. 2b) and the EPI image of brain  $T_1$  relaxation times (Fig. 2d). The mean cerebral blood flow value in the slice is 65 cc/100 g/min.

A histogram of the cerebral blood flow values in the slice is shown in Fig. 4. Figure 4 does not show a bimodal distribution that might be expected from the threefold difference in mean cerebral blood flow values observed for gray and white matter (12). Two explanations for this observation could be that the blood flow values within either gray matter or white matter have a wide distribution (13), or that differences in blood flow between white and gray matter are obscured by partial volume effects.

#### Reproducibility of Cerebral Blood Flow Images

The cerebral blood flow image shown in Fig. 2e was calculated by averaging three consecutive cerebral blood flow images. Each image was calculated from data acquired in approximately 8 min. The three consecutive blood flow images are shown in Fig. 5. The average correlation coefficient (14),  $r$ , between single-voxel blood flow values in consecutive images was 0.85. Qualita-

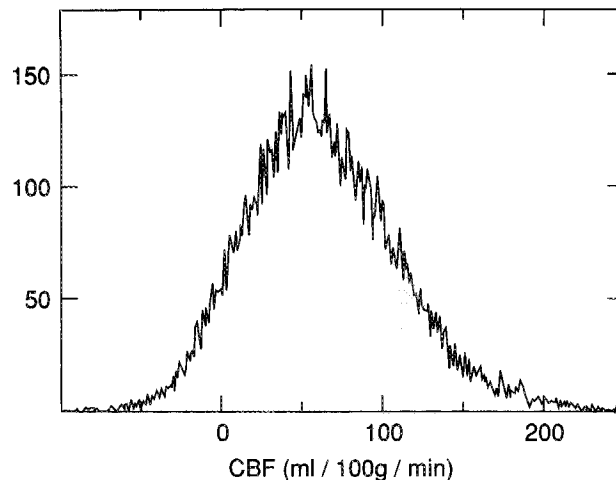


FIG. 4. Histogram of cerebral blood flow values from the image shown in Fig. 2e. The vertical scale corresponds to the number of voxels having a specific cerebral blood flow value. A 1-cc/100 g/min range was used to "bin" the cerebral blood flow data.

tively, most of the features of the cerebral blood flow maps are reproduced in the three images.

#### Artifacts in the Cerebral Blood Flow Image

The cerebral blood flow images shown in Figs. 2e and 5 show two types of artifacts. First, the images contain "bright" spots that have apparent cerebral blood flow values far above expected values (e.g.,  $\geq 200$  cc/100 g/min) (15). Comparison of the location of these "bright" spots with a SPGR image (see Fig. 2c) shows that many of these artifacts appear near large vessels.

The images shown in Figs. 2e and 5 also contain a number of voxels with apparently negative cerebral blood flow values. These voxels appear as black spots in the cerebral blood flow maps. The histogram shown in Fig. 4 indicates that, for the data shown in Fig. 2e, approximately 14% of the voxels have apparently negative cerebral blood flow values. The interpretation of the negative cerebral blood flow values is unclear (see Discussion).

#### Summary of Spin Tagging Experiments

Spin tagging experiments were performed on a total of six subjects. All subjects showed cerebral blood flow maps that gave clear contrast between gray and white matter regions, and all of the histograms of cerebral blood flow values were similar to that shown in Fig. 4. Also, all of the histograms of  $T_1$  values were similar to that shown in Fig. 3. Average cerebral blood flow values and  $T_1$  values for the different subjects are shown in Table 1. For the six subjects, the mean value of the average cerebral blood flow in the slice was  $51 \pm 11$  cc/100 g/min.

All subjects showed at least some "bright" artifacts in regions that corresponded to large vessels. The average fraction of voxels showing apparent blood flow values over 200 cc/100 g/min was 2.0%. Also, all subjects showed voxels with apparently negative cerebral blood flow values. The average fraction of voxels showing negative cerebral blood flow values was 17%.

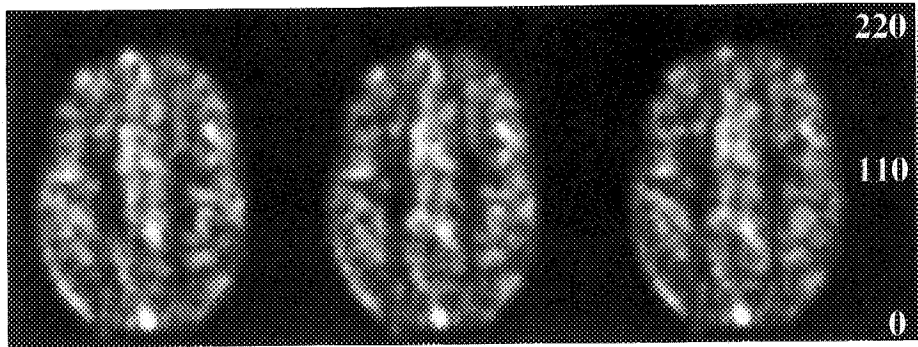


FIG. 5. Three cerebral blood flow images taken consecutively on a subject during the same experiment. The data for each image took 7 min to acquire. Negative cerebral blood flow values (see text) were replaced by zero before the images were interpolated and Gaussian "smoothed."

Table 1  
Average Longitudinal Relaxation Time,  $\langle T_1 \rangle$  and Cerebral Blood Flow,  $\langle Q \rangle$ , for Six Normal Subjects

	Subject					
	1	2	3	4	5	6
$\langle T_1 \rangle$ (sec)	1.19	1.17	1.37	1.31	1.23	1.25
$\langle Q \rangle$ (cc/100 g/min)	65	51	55	57	33	44

$\langle T_1 \rangle$  is the average water longitudinal relaxation time calculated for the slice indicated in Fig. 2.  $\langle Q \rangle$  is the average cerebral blood flow calculated for the slice indicated in Fig. 2. The position of the slice varied slightly from subject to subject.

#### Errors in Calculated Cerebral Blood Flow Values

The cerebral blood flow values calculated using Eq. [1] have two sources of random statistical error. The major source is statistical error in the calculated values of  $\Delta M/M_0$  for individual voxels. An estimate of this error can be calculated from the standard deviation of  $\Delta M/M_0$  values observed for a single four-step cycle ( $\sim 1.9\%$ ). The standard error of the mean value of  $\Delta M/M_0$  averaged over the 39 four-step cycles would thus be  $\sim 0.30\%$ . Assuming an average  $T_1$  of 1 s, the average precision of cerebral blood flow values calculated from the 8-min data acquisition was approximately  $\pm 10$  cc/100 g/min.

The second source of random statistical error in the calculated cerebral blood flow values is the  $T_1$  relaxation rate. The reproducibility of the single-voxel  $T_1$  values for the three separate determinations (see Materials and Methods) was approximately  $\pm 3\%$ . This random error in calculated  $T_1$  values would contribute an error of approximately  $\pm 3\%$  to the calculated values of cerebral blood flow, and thus is negligible.

#### DISCUSSION

One of the major problems with arterial spin tagging approaches is the sensitivity to instrumental instabilities and head motion. The aim of the work presented here was to demonstrate that fast imaging techniques such as single-shot EPI can reduce the sensitivity of spin tagging approaches to instrumental instabilities and head motion, and can provide reproducible cerebral blood flow images in humans at 1.5 T.

The major advantage of single-shot EPI techniques is that a complete image of  $\Delta M/M_0$  can be obtained, using the four-step cycle, in approximately 8 s. Even though the  $\Delta M/M_0$  data acquired in a single four-step cycle were averaged over 39 cycles to obtain adequate signal-to-

noise, the short "performance time" of a single four-step cycle meant that artifacts in the calculated value of  $\Delta M/M_0$  due to instrumental drift were substantially reduced.

Another advantage of the single-shot EPI technique is that  $T_1$  images can be obtained in less than 3 min. The  $T_1$  image and the  $\Delta M/M_0$  image can thus both be acquired in 8 min. The short acquisition time for the pair of images substantially reduces the possibility of misregistration between  $T_1$  images and the  $\Delta M/M_0$  images due to head motion, and thus substantially reduces systematic errors in the calculation of cerebral blood flow images using Eq. [1].

One way to assess the efficacy of EPI techniques in reducing systematic errors in the spin tagging approach is to investigate the reproducibility of cerebral blood flow images. The data shown in Fig. 5 can be used to show that consecutive cerebral blood flow images taken at the same examination are reproducible (see Results section), and support the importance of fast imaging techniques in acquiring spin tagging data.

Single-shot EPI techniques do, however, have a number of disadvantages for imaging cerebral blood flow with spin tagging approaches. First, they have relatively poor spatial resolution compared with "high-resolution" MR images. For example, the  $64 \times 64$  images presented here have a nominal in-plane resolution of 3.75 mm, which is similar to the resolution found in PET images. While part of the limitation in spatial resolution is inherent in the EPI technique (7-9), part is due to the poor signal-to-noise of the spin tagging approach. Another disadvantage of the single-shot EPI technique is distortion of the images due to susceptibility effects (7-9).

The cerebral blood flow images shown in Figs. 2e and 5 show two artifacts that must be overcome before spin tagging approaches can be used for routine clinical studies. The first artifact is the presence of "bright spots" located near large vessels, which can give apparent cerebral blood flow values that are unreasonably large. The pulse sequence used for these experiments has large gradients placed symmetrically around the  $180^\circ$  pulse to "crush" signals from moving spins. However, while signals from small arteries that are randomly distributed within a voxel will be attenuated, signals from large arteries will experience a phase shift. The contribution to the steady-state value of  $\Delta M/M_0$  from inverted water spins in large arteries will increase the apparent cerebral blood flow in the voxel. Signals from rapidly moving blood in large arteries can be directly visualized using

"dynamic" tagging approaches such as EPSTAR (16, 17) or selective/nonselective slice inversion (18, 19).

It is interesting that the sagittal sinus appears bright on Fig. 2e. A similar finding was observed using EPSTAR approaches by Edelman *et al.* (16), who suggested that it may be due to tagging of ascending venous blood in the anterior segment of the sagittal sinus. The same explanation could also be true in our experiments, although under our conditions the tagging plane may not be high enough to reach a significant portion of the anterior sagittal sinus (see Fig. 1). However, other veins that ascend through the tagging plane and drain into the superior sagittal sinus could also cause tagging of sagittal sinus blood by this mechanism.

The second artifact in the cerebral blood flow images is the presence of voxels with apparently negative cerebral blood flow values (see Fig. 4). Voxels localized in brain regions with very low blood flow, e. g., cerebrospinal fluid, could have apparently negative blood flow values due to statistical deviations in the blood flow measurement ( $\pm 10$  cc/100 g/min, see Results section). It is unclear if statistical variation can explain all the the negative values observed in Fig. 4. However, voxels that contain veins with retrograde flow could also have apparently negative blood flow values because water spins in these veins could be inverted during the control part of the four-step cycle, instead of the inversion part of the cycle.

For the six subjects, the mean value of the average cerebral blood flow in the slice was  $51 \pm 11$  cc/100 g/min, which is in good agreement with average global cerebral blood flow values determined in humans using the Kety-Schmidt approach, i.e.,  $\sim 55$  cc/100 g/min (20). However, this close agreement is probably fortuitous, for the following reasons. First, measured  $\Delta M/M_0$  values may still have a contribution from tagged arterial spins that were not completely dephased by the crusher gradients, and, second, longitudinal relaxation during arterial transit may decrease  $\alpha$ . The first effect could cause an over-estimate of cerebral blood flow, while the second could cause an under-estimate of cerebral blood flow. The two errors tend to cancel, and thus may not be apparent. Clearly, reliable quantitation of cerebral blood flow using arterial spin tagging approaches requires accurate correction for both errors.

If the systematic errors discussed above can be circumvented, the statistical precision of the calculated cerebral blood flow values should be approximately  $\pm 10$  cc/100 g/min for an 8-min scan (see Results). One way to improve the precision might be to work at higher magnetic field strengths. One advantage of higher field strengths is that the intrinsic signal-to-noise ratio may be higher. Another advantage is that the longer  $T_1$  observed at higher field strengths (21) will give a larger  $\Delta M/M_0$  (see Eq. [1]), but this advantage is partly (but not completely) balanced by the fact that the longer  $T_1$  will decrease the effective signal-to-noise (22). A potential disadvantage with high magnetic field strengths is that increased RF power absorption at higher field strengths (23) will reduce the maximum amplitude of the off-resonance RF irradiation. Given the number of factors involved, the

optimum field strength for arterial spin tagging experiments is not clear.

The spin tagging technique described here uses a single coil both to tag arterial spins and to map cerebral blood flow in the imaging slice (see Fig. 1). RF pulses used to generate arterial tagging (2) thus produce magnetization transfer effects in the imaging slice (24). The procedure used to correct for magnetization transfer effects is not easily applicable to multislice imaging approaches, which effectively restricts the single-coil technique to single-slice cerebral blood flow images. This restriction could be circumvented if arterial blood was tagged at the neck with a second coil, which would minimize magnetization transfer effects (25, 26). However, under these conditions, the increased transit time from the tagging plane to tissue in the imaging slice might substantially decrease the observed values of  $\Delta M/M_0$ . Correction for the decrease in  $\Delta M/M_0$  due to longitudinal relaxation during arterial transit would require a measurement of the arterial transit time.

In summary, single shot EPI techniques can be used to reduce the sensitivity of arterial spin tagging approaches to instrumental instabilities and head motion. While EPI/arterial spin tagging approaches allow the calculation of reproducible cerebral blood flow images in humans in 8 min at 1.5 T, a number of "blood volume" artifacts in the image must be overcome before the approach can be applied to routine clinical studies.

## ACKNOWLEDGMENTS

The authors thank Dr. Daniel Weinberger for helpful discussions and for support of this work, and Drs. Peter van Gelderen and Chrit Moonen for helpful discussion on spatial resolution and point-spread functions. This work was performed at the NIH In Vivo NMR Research Center.

## REFERENCES

1. J. A. Detre, J. S. Leigh, D. S. Williams, A. P. Koretsky, Perfusion imaging. *Magn. Reson. Med.* **23**, 37-45 (1992).
2. D. S. Williams, J. A. Detre, J. S. Leigh, A. P. Koretsky, Magnetic resonance imaging of perfusion using spin inversion of arterial water. *Proc. Natl. Acad. Sci. USA* **89**, 212-216 (1992).
3. E. G. Walsh, K. Minematsu, J. Leppo, S. C. Moore, Radioactive microsphere validation of a volume localized continuous saturation perfusion measurement. *Magn. Reson. Med.* **31**, 147-153 (1994).
4. J. R. Ewing, J. M. Boska, Y. Cao, S. Brown, Z. G. Zhang, K. M. A. Welch, A fast method for measuring cerebral perfusion using arterial spin labeling and variable flip-angle FLASH imaging, in "Proc., SMR, 3rd Annual Meeting, Nice, France, 1995," p. 871.
5. J. Pekar, P. Jezzard, D. A. Roberts, J. S. Leigh, J. A. Frank, A. C. McLaughlin, Perfusion imaging with compensation for asymmetric magnetization transfer effects. *Magn. Reson. Med.* **35**, 70-79 (1996).
6. D. A. Roberts, J. A. Detre, L. Bolinger, E. K. Insko, J. S. Leigh, Quantitative magnetic resonance imaging of human brain perfusion at 1.5 T using steady-state inversion of arterial water. *Proc. Natl. Acad. Sci. USA* **91**, 33-37 (1994).
7. J. Pekar, P. Jezzard, J. H. Duyn, J. A. Frank, A. C. McLaughlin, Echo planar perfusion imaging with MTC offset compensation in normal volunteers, in "Proc., SMR, 3rd Annual Meeting, Nice, France, 1995," p. 884.
8. P. Mansfield, Multiplanar image formation using NMR spin echoes. *J. Phys. C* **10**, L55-58 (1977).
9. M. K. Stehling, R. Turner, P. Mansfield, Echo-planar imaging: mag-

- netic resonance imaging in a fraction of a second. *Science* **254**, 43-50 (1991).
10. R. Turner, P. Jezzard, Magnetic resonance studies of brain functional activation using echo-planar imaging, in "Functional Neuroimaging: Technical Foundations" (R. W. Thatcher, M. Hallett, T. Zeffiro, E. R. John, M. Heurta, Eds.), pp. 69-78, Academic Press, San Diego, 1994.
  11. P. Herscovitch, M. E. Raichle, What is the correct value for the brain-blood partition coefficient for water? *J. Cereb. Blood Flow Metab.* **5**, 65-69 (1985).
  12. R. S. J. Frackowiak, G-L. Lenzi, T. Jones, J. D. Heather, Quantitative measurement of regional cerebral blood flow and oxygen metabolism in man using  $^{15}\text{O}$  and positron emission tomography: theory, procedure, and normal values. *J. Comput. Assist. Tomogr.* **4**, 727-736 (1980).
  13. D. H. Ingvar, N. A. Lassen, Regional blood flow of the cerebral cortex determined by Krypton $^{85}$ . *Acta Physiol. Scand.* **54**, 325-338 (1962).
  14. P. R. Bevington, "Data Reduction and Error Analysis for the Physical Sciences," p. 121, McGraw-Hill, New York, 1969.
  15. K. Herholz, U. Pietrzyk, K. Wienhard, I. Hebold, G. Pawlik, R. Wagner, V. Holthoff, P. Klinkhammer, W-D. Heiss, Regional cerebral blood flow measurement with intravenous [ $^{15}\text{O}$ ] water bolus and [ $^{18}\text{F}$ ] fluoromethane inhalation. *Stroke* **20**, 1174-1181 (1989).
  16. R. R. Edelman, B. Siewert, D. G. Darby, V. Thangaraj, A. C. Nobre, M. M. Mesulam, S. Warach, Qualitative mapping of cerebral blood flow and functional localization with echo-planar MR imaging and signal targeting with alternating radio frequency. *Radiology* **192**, 513-520 (1994).
  17. R. B. Buxton, L. R. Frank, B. Siewert, S. Warach, R. R. Edelman, A quantitative model for EPSTAR perfusion imaging, in "Proc., SMR, 3rd Annual Meeting," Nice, France, 1995, p. 132.
  18. S-G. Kim, Quantification of relative cerebral blood flow change by flow-sensitive alternating inversion recovery (FAIR) technique: application to functional mapping. *Magn. Reson. Med.* **34**, 293-301 (1995).
  19. K. K. Kwong, D. A. Chesler, R. M. Weisskoff, K. M. Donahue, T. L. Davis, L. Ostergaard, T. A. Campbell, B. R. Rosen, MR perfusion studies with  $T_1$ -weighted echo planar imaging. *Magn. Reson. Med.* **34**, 878-887 (1995).
  20. B. K. Siesjo, "Brain Energy Metabolism," p. 74, John Wiley, New York, 1978.
  21. G. D. Fullerton, Physiologic basis of magnetic relaxation, in "Magnetic Resonance Imaging" (D. D. Stark, W. G. Bradley, Eds.), 2nd ed., pp. 88-108, Mosby Year Book, St. Louis, 1992.
  22. R. R. Ernst, W. A. Anderson, Application of Fourier transform spectroscopy to magnetic resonance. *Rev. Sci. Instr.* **37**, 93-102 (1966).
  23. C-N. Chen, D. I. Hoult, "Biomedical Magnetic Resonance Technology," pp. 127-132, Adam Hilger, Bristol, 1989.
  24. W. Zhang, D. S. Williams, J. A. Detre, A. P. Koretsky, Measurement of brain perfusion by volume-localized NMR spectroscopy using inversion of arterial water spins: accounting for transit time and cross-relaxation. *Magn. Reson. Med.* **25**, 362-371 (1992).
  25. J. A. Detre, W. Zhang, D. A. Roberts, A. C. Silva, D. S. Williams, D. J. Grandis, A. P. Koretsky, J. S. Leigh, Tissue specific perfusion imaging using arterial spin labeling. *NMR Biomed.* **7**, 75-82 (1994).
  26. W. Zhang, A. C. Silva, D. S. Williams, A. P. Koretsky, NMR measurement of perfusion using arterial spin labeling without saturation of macromolecule spins. *Magn. Reson. Med.* **33**, 370-376 (1995).